Surface oscillations of a liquid-solid fluidized bed

Loïc Rousseau, Laurence Girolami, Mohammed Boussafir, Frédéric Risso

Surface oscillations of a liquid-solid fluidized bed

Loïc Rousseau[1], Laurence Girolami[1,2], Mohammed Boussafir[1], and Frédéric Risso[3]

[1] *GéHCO, Université de Tours, Campus Grandmont, 37200 Tours, France*

[2] *RECOVER, INRAE-Aix-Marseille Université,*

13100 Aix-en-Provence, France and

[3] *Institut de Mécanique des Fluides de Toulouse (IMFT),*

Université de Toulouse, CNRS, 31400 Toulouse, France

(Dated: January 6, 2026)

Abstract

We report experimental investigations of an unconfined liquid-solid fluidized bed at low to moderate Reynolds number. The fluidization velocity U_f is measured when an upward flow is imposed, and the sedimentation velocity U_{sed} is measured when the flow is stopped. Only when the level of inlet flow fluctuation is sufficiently low will these two velocities coincide, as expected for an unbound system. A systematic comparison between U_f and U_{sed} should therefore be made when attempting to determine fluidization laws. Comparisons with previous studies show that U_f measurements gather on a single function of the ratio Φ/Φ_{pack} between the particle volume fraction Φ and its packing value Φ_{pack}, except for a factor K that encompasses all effects other than concentration: Stokes number, Reynolds number, confinement and inlet condition. Time-resolved measurements of the fluidized bed surface show two contributions: uncorrelated high-frequency fluctuations and low-frequency oscillations that remain correlated over minutes. The coherent oscillations correspond to the arrival of upward concentration waves at the bed surface. Their wavelength, which characterizes the length scale of large-scale heterogeneities, was known to diverge as the packing state is approached. Here, we found that it also increases with decreasing concentration, suggesting that the loss of global bed stability observed in previous work at high expansions may be related to the development of heterogeneous structures of a size comparable to that of the column.

I. INTRODUCTION

Dispersed two-phase media, consisting of a population of particles immersed in a fluid, are very common in industrial and natural flows. A key mechanism of their dynamics is the resistance to the motion of the particles through the fluid, which can be seen as an increase of the drag force on the particles due to the presence of their neighbors. When the particles are uniformly distributed in space, the drag increases with the particle concentration because of the enhanced shear in the interstices between the particles. This phenomenon, known as the hindrance effect, can be isolated in two configurations that are particularly well suited to its investigation. In the case of particles that are heavier than the fluid, those are: the fluidization of the particles by a uniform ascending flow or their sedimentation through a fluid at rest. As noted by Batchelor in 1988 [1], assuming there is no significant wall effect, those two situations are symmetric. We will examine both situations here, although even

today their study is still divided in the literature. We refer to the average fluidization velocity as U_f and the average sedimentation velocity as U_{sed}, or we use U for both when the difference is irrelevant.

The simplest situation is that of a uniform suspension of identical solid particles of density ρ_p and equivalent diameter d, in a Newtonian fluid of density ρ_f and viscosity μ_f. In that case, the dynamics can be reasonably characterized by four dimensional parameters: a Reynolds number, $Re = \frac{\rho_f U d}{\mu_f}$, comparing fluid inertia to viscous forces, a Stokes number, $St = \frac{(\rho_p + 1/2\rho_f) U d}{\mu_f}$, comparing particle inertia to viscous forces, the current particle volume fraction Φ, and the particle volume fraction Φ_{pack} in the loose packing state reached after particles have settled. The latter should not be forgotten, as it determines the volume fraction at which the sedimentation velocity becomes zero. Many attempts have been made to find a fluidization/sedimentation law, $U(\Phi)$. Very often, experimental results are adjusted by the original Richardson-Zaki empirical correlation [2], $U = U_i(1 - \Phi^n)$, which can be improved as $U = U_i(1 - \Phi/\Phi_{pack})^n$ by including Φ_{pack}. If such correlations most of the time provide reasonable agreement with experimental data in an intermediate range of values of Φ, no general relationship between U_i and n and the various non-dimensional groups has been achieved.

In a previous work [3], some of the authors investigated the fluidization and the sedimentation of 8 types of particles in two fluids, water at 20°C and 35°C (to vary the viscosity) and air at 170°C (to cancel inter-particle cohesion due to moisture). The experiments were conducted in unconfined condition with a ratio between the particle and the container sizes between 600 and 3000. The particle Reynolds number was small to moderate ($6 \times 10^{-3} \leq Re \leq 4$) while the Stokes number was small to large ($1.5 \times 10^{-2} \leq St \leq 70$). The smallest Re and largest St were obtained with volcanic ash particles in air, thanks to their small size ($d \leq$100 μm) and very large density ratio. The smallest St was reached with light PMMA particles in water, and the larger Re with 335 μm heavy glass beads in water. Velocities U_f and U_{sed} were systematically measured in a range of volume fraction between two limits, Φ_{low} and Φ_{up}, that depend on the system under consideration. At $\Phi = \Phi_{pack}$, the particles cease settling ($U_{sed} = 0$), while the liquid can still go through the bed ($U_f \neq 0$). Φ_{up} was defined as the volume fraction from below which $U_{sed} = U_f$, its value ranging from 0.80 to 0.95 Φ_{pack}. In between Φ_{low} and Φ_{up}, the surface of the bed is easy to locate and approximately horizontal, while below Φ_{low} the surface becomes diffuse and difficult to define.

Φ_{low} was thus associated with the limit of stability of a homogeneous suspension. The terms "stable" and "homogeneous" have to be taken with care. In that case, the homogeneity was not only justified by the fact that the interface was approximately flat, but also by the fact that $U_{sed} = U_f$, which implied that the lateral walls did not affect the flow motion. The expression "limit of stability" was justified by the fact that a sudden transition towards a visually inhomogeneous state was observed at Φ_{low}. It is worth mentioning that the value of Φ_{low} was found to increase with the Stokes number, which characterizes the importance of particle inertia. The larger the Stokes number, the narrower the concentration range $[\Phi_{low}, \Phi_{pack}]$ where the homogeneous regime was observed. In this regime, the results of all the systems considered were well described by a single correlation

$$U = \frac{U_0(1-\Phi)}{F(\frac{\Phi}{\Phi_{pack}})K(St_0)}\,, \tag{1}$$

where $U_0 = \frac{(\rho_p - \rho_f)gd^2}{18\mu_f}$ is the Stokes velocity for an isolated particle and $St_0 = \frac{(\rho_p + 1/2\rho_f)(\rho_p - \rho_f)gd^3}{18\mu_f^2}$ is the Stokes number based on U_0. F is a function that increases from 1 to ∞ as of Φ/Φ_{pack} increases from 0 to 1. It is exponential at low Φ and diverges as a power law similar to the Richardson-Zaki law when approaching the packing state. It describes the hindering effect for a system at negligible particle inertia. K is a function that increases from 1 to 3 as St_0 increases from 0 to ∞. It describes the fact that the hindering effect is enhanced by the inertia of the particle. Most of the experimental results having been obtained at small Reynolds number, the effect of Re is not accounted for in eq. (1), which should be understood as the low Re limit of that sedimentation/fluidization law.

Experiments by [4] have shown that particle inertia also reduces the threshold for the onset of concentration waves, which are considered to be the first step towards complete bed destabilization [5]. The significant effect of particle inertia on both U and the suspension homogeneity means that fluctuations take an important role upon the suspension dynamics, even in the limit of small Re. It is thus highly desirable to characterize such fluctuations and to understand how are related average velocity U and concentration fluctuations, and global stability of the homogeneous state. Unfortunately, the presence of numerous solid/fluid interfaces makes the suspension opaque and complicates measurements within it. Some optical techniques can be used, depending on the ratio w/d between the container thickness w and the particle size d. Measuring the intensity of a laser beam passing through the suspension, Ham et al. (1990) [4] detected concentration waves for $10 < w/d < 50$. Filming

neon light transmitted through the suspension, Duru et al. (2002) [6] made maps of the concentration average over the gap for $w/d \approx 17$, which enabled the characterization of non-planar waves. Using optical index matching between transparent beads and the suspending fluid, Alméras et al (2021) [7] measured the velocity fluctuations of both the fluid and the particles for $w/d \approx 13$. However, there is a lack of results regarding concentration and velocity fluctuations in unconfined situations. That means that particles are much smaller than the container, let's say $w/d \geq 100$, but the confinement ratio would be better defined from the scale Λ of the larger inhomogeneities, as $\Lambda/w \gg 1$.

The present study is an experimental investigation of fluidized/sedimented suspensions, considering the same particles and fluid as Ref. [3], but a different injection system. We have chosen to focus on unconfined systems ($w/d \geq 500$) at the cost of limiting our investigation to measurements of the bed surface motions, which are analyzed using statistical and spectral tools to provide insights into the mean velocity, magnitude and time scales of the fluctuations. The results are compared to previous studies of confined suspensions for which average sedimentation velocity and concentration-wave properties have been measured [4, 8–10]. The paper is organized as follows: experimental setup and procedures are described in section II, sedimentation and fluidization laws are examined in section III, spatio-temporal fluctuations of the suspension surface are investigated in section IV, the spatially-averaged time oscillations of the fluidized bed height are analyzed and discussed with respect to their connection with concentration waves in section V, concluding remarks are given in section VI.

II. EXPERIMENTAL SETUP AND MEASUREMENTS TECHNIQUES

Three types of particles are investigated (see Table I): two sets of glass beads of diameter 160 μm (GB1) or 335 μm (GB3) and one set of PMMA beads of 210 μm. They are immersed in tap water at ambient temperature, ranging between 18℃ and 25℃. The three sets have been chosen to show contrasting inertial effects. With PMMA particles, both the Reynolds and Stokes numbers are low. With GB1, Re remains below 1.1 while St significantly exceeds unity. With GB3, Re is greater than 1 and St greater than 2.8.

The experimental setup is depicted in Fig. 1a. It consists of a vertical reservoir made of PMMA of 900 mm height with a rectangular cross section of dimension w_1=200 mm in

Parameters	$GB1$	$GB3$	$PMMA$
d [μm]	160	335	210
ρ_{p} [kg m^{-3}]	2500	2500	1200
ρ_{f} [kg m^{-3}]	998	998	998
μ_{f} [$10^{-3}Pa.s$]	[0.833, 1.109]	[0.967, 1.081]	[1.015, 1.095]
h_0 [m]	0.18	[0.35, 0.48]	0.09
h_{mid} [m]	[0.21, 0.44]	0.54	[0.12, 0.21]
ϕ_{pack}	0.59	0.59	0.59
$\phi_s/\phi_{pack} = 1/E$	[0.41, 0.86]	[0.65, 0.89]	[0.43, 0.73]
$St_0 = \frac{(\rho_p+1/2\rho_f)(\rho_p-\rho_f)gd^3}{18\mu_f^2}$	[9.5, 14.5]	[78, 94]	[1.4, 1.7]
U_f [mm s^{-1}]	[1.1, 6.0]	[3.1, 8.9]	[0.37, 1.04]
$Re = \frac{\rho_f U_f d}{\mu_f}$	[0.19, 1.1]	[0.95, 2.8]	[0.05, 0.22]
$St = \frac{(\rho_p+1/2\rho_f)U_f d}{\mu_f}$	[0.5, 3.4]	[2.9, 8.3]	[0.11, 0.37]

TABLE I. Particles and fluid physical parameters, as well as ranges of operating conditions. Note that the viscosity of the water varies between the different tests due to slight variations in temperature.

the x direction, and w_2=300 mm in the y direction. (Note that the column consists of two connected segments. The connection is smooth and has no effect on the flow within the column. However, it prevents measurements being taken in the range of elevations from 250 mm to 280 mm.)

In fluidization mode, water is supplied by a pump and injected from below through a porous medium, whose role is to homogenize the flow. The four-blade centrifugal pump rotates at speeds between 2,500 and 3,000 rpm, powered by a 50 Hz electrical current. The cyclic nature of the pump may generate low-amplitude fluctuations at frequencies greater than 40 Hz. The porous medium is made of three layers topped by a mesh filter that held them in place: one layer of gravels of roughly 4 mm diameter, one layer of 4 mm iron beads mixed up with 0.336 mm glass beads, covered with a 10-mm thick sponge.

A mass m_p of particles is introduced into the water-filled column. The pump is started and the flow rate Q_{flow} is adjusted. Q_{flow} is measured by means of an electromagnetic flow meter, from which is determined the sedimentation velocity $U_f = Q_{\mathrm{flow}}/(w_1 w_2)$, with an

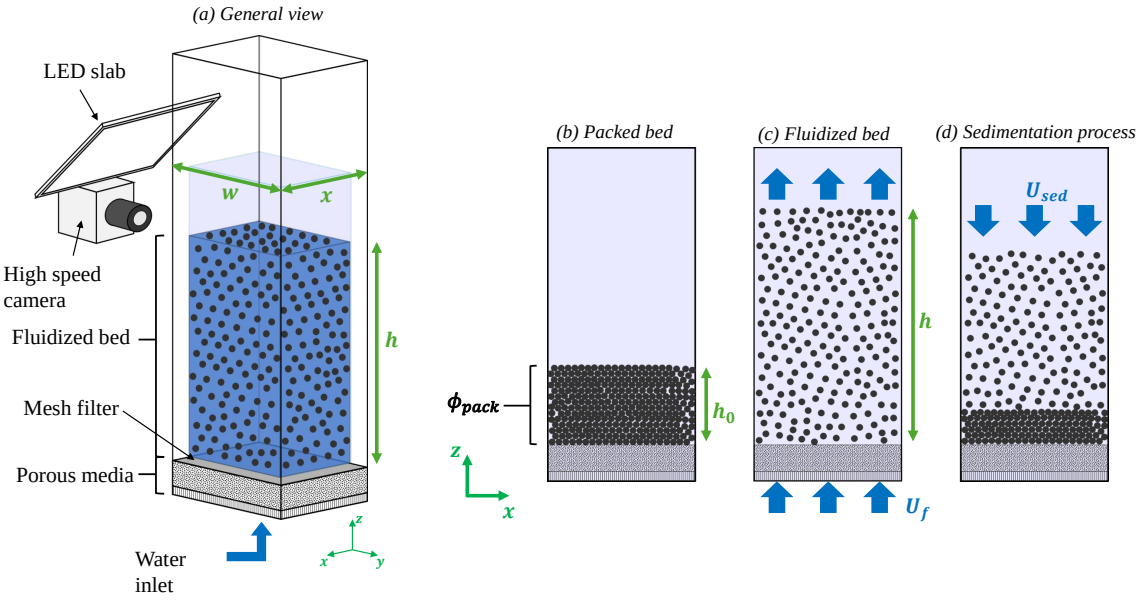

FIG. 1. Experimental setup. (a) General view, (b) Packed state after sedimentation, (c) steady state during fluidization, (d) Sedimentation process.

FIG. 2. Snapshots of the bed surface at various concentrations during fluidization.

accuracy of $\pm 2\%$. After a short transient, the bed of particles reaches steady state (Fig. 1b) and its height h_{mid} is measured by means of a ruler located in the middle of the shorter face of the the column, at $x = x_{mid} = w_1/2$. Then, the water supply is stopped and the particles settle (Fig. 1c) until they form a steady deposit of height h_0 and solid volume concentration $\Phi_{pack} = m_p/(\rho_p h_0 w_1 w_2)$, which corresponds to a loose random packing associated with the

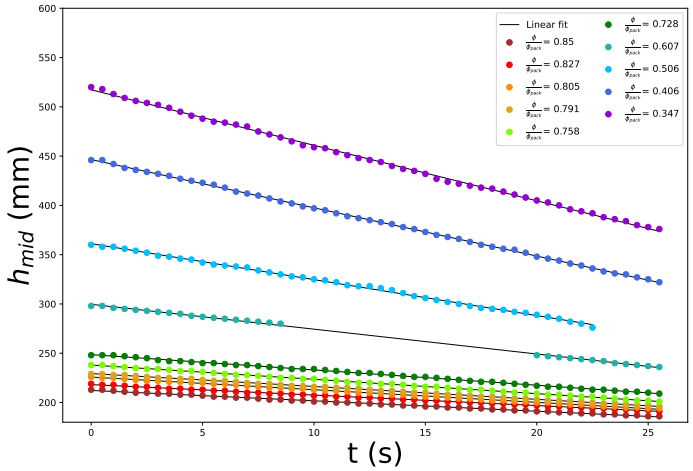

FIG. 3. Time evolution of the bed height $h_{mid}(t)$ at the middle of the column during bed collapse experiments. (The lack of data for the case at $\Phi/\Phi_{pack} = 0.607$ is due to the passage of the interface at a junction of the column.)

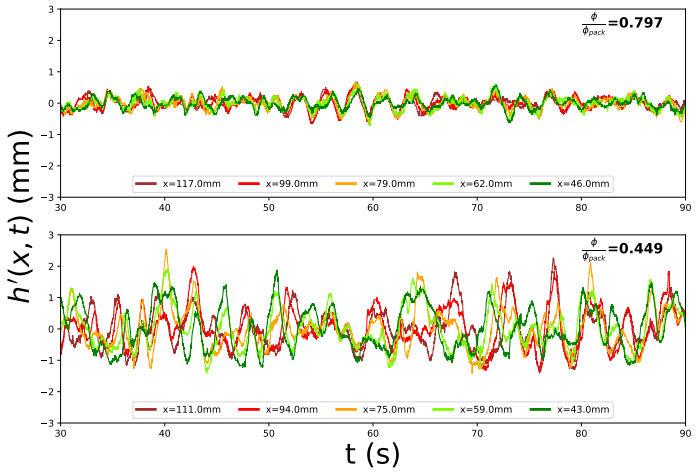

FIG. 4. Bed height time fluctuations $h'(x,t)$ at various distance x from the wall during fluidization experiments.

microstructure of the fluidized bed. The bed expansion $E = h_{mid}/h_0$ of the fluidized bed is measured with an accuracy of $\pm 2\%$ and its solid concentration Φ is determined through the relation $\Phi/\Phi_{pack} = 1/E$.

The surface of the bed is illuminated by a LED panel located above and inclined at 45 degrees to the vertical, and filmed by means of a Phantom VE-O 340L camera located on the same side of the column. The camera has an horizontal viewing axis and focuses on the

bed surface near to the wall. It images a rectangular window of the (x,z) plane from the left wall ($x_{wall} = 0$) to a point located 20 mm from the column middle ($x_{max} = 120$ mm), with a resolution of 16 pixels per millimeter. Examples of images are provided in Fig. 2. During bed collapse, the camera is operated at 1200 frames per second and the time evolution of the bed height at the middle of the column, $h_{mid}(t)$, is determined. Fig. 3 shows the result for GB1 particles at various concentrations. We observe small oscillations around a linear decay. The fact that the average velocity does not change confirms that the average solid concentration remains unchanged throughout the process. The presence of regular oscillations is reminiscent of the traveling waves observed in the previous works mentioned in the introduction. During fluidization, the acquisition rate is set to 150 frames per second and the spatio-temporal profile of the surface, $h(x,t)$, between x_{wall} and x_{max} is extracted by image processing. In what follows, time averaging is denoted by an overbar, $\bar{}$, and space averaging by brackets, $\langle\ \rangle$.

Fig. 4 presents the time fluctuations, $h'(x,t) = h(x,t) - \overline{h(x,t)}$, for GB1 particles at various distances x from the wall for two different solid fractions. The signal shows variation of amplitude less than 2 mm and involves both a regular oscillation and random fluctuations. Its characteristics do not change with time, which means that it is statistically steady, but depends on Φ. In what follows, the analysis of surface fluctuations will be carried out on fluidization experiments, whose signals are better suited to processing because they are not limited to a short duration, unlike collapse tests.

III. SEDIMENTATION AND FLUIDIZATION VELOCITIES

In this section, we examine the average fluidization and sedimentation velocities, before considering interface fluctuations in the next sections. Fig. 5 presents the measured values of U_f and U_{sed} as a function of the normalized concentration Φ/Φ_{pack}, for the three sets of particles. Our results (circles) are compared with those of Ref. [3] (squares) for the same particles. As expected, U_f and U_{sed} are decreasing functions of Φ/Φ_{pack} and are lower the lighter or smaller the particles.

Comparing U_f to U_{sed}, Ref. [3] found that sedimentation and fluidization velocities remained equal over the concentration range studied. Our results show different features depending on the type of particles considered. For PMMA particles, U_f and U_{sed} remain

equal over the concentration range studied. For GB1, they are still close at high concentration but U_f becomes greater than U_{sed} for $\Phi/\Phi_{pack} \leq 0.6$. For GB3, U_f is always greater than U_{sed} and the discrepancy increases when decreasing the concentration. Compared to Ref. [3], the present particles and column are the same, but the porous medium through which water is injected is significantly less compact. In our case, it is therefore likely that disturbances in the upstream flow are stronger and less filtered by the porous medium. In Ref. [3], incoming fluctuations are negligible compared to the fluctuations that are naturally present in a suspension due to the interactions between particles. The result is that the fluidization process, where the pump is running, is not different from the sedimentation process, where the pump is switched off. In the present work, additional disturbances during fluidization cause an increase of U_f. The effect of the injection condition that has been revealed here highlights the difficulty of quantitative comparisons between fluidization velocities measured in different setups of the literature.

We now compare fluidisation velocities obtained by different authors for different types of particles, which requires making U_f dimensionless. A way to do that is to define the relative sedimentation viscosity of the suspension as

$$\frac{\mu_{sed}}{\mu_f} = \frac{U_0(1-\Phi)}{U_f}\,, \tag{2}$$

where μ_{sed} is the viscosity of an equivalent fluid having the same density, $\rho_m = (1-\Phi)\rho_f + \Phi\rho_p$, of the suspension, in which a single particle settles at a velocity U_f in the limit of vanishing Reynolds number [11]. Using Eq. (2), Eq. (1) can be recast as follows

$$\frac{\mu_{sed}}{\mu_f} = K\,F(\frac{\Phi}{\Phi_{pack}})\,, \tag{3}$$

where K is a coefficient that takes into account the effect of particle inertia, which can be expressed as a function of only St_0 when the Reynolds number is small, the suspension is unconfined and homogeneous, and the inlet condition does not affect the dynamics ($U_{sed} = U_f$). In Fig 6 are plotted the values of $F = \mu_{sed}/(K\mu_f)$ as the function of Φ/Φ_{pack} for the present work as well as for experiments of Ref. [3, 4, 8–10], whose physical properties are reported in Table II. A value of K has been adjusted for each series so as to collapse the data on the following empirical curve [12],

$$F_{fit}(\frac{\Phi}{\Phi_{pack}}) = \exp(1.9\frac{\Phi}{\Phi_{pack}}) + 0.85(\frac{\Phi}{\Phi_{pack}})^2(1-\frac{\Phi}{\Phi_{pack}})^{-2/3}\,. \tag{4}$$

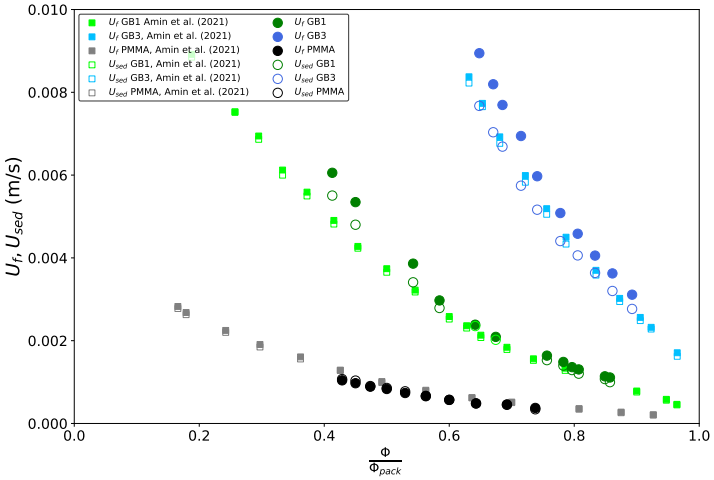

FIG. 5. Fluidization and sedimentation velocity measured for all sets of particles as a function of the particle concentration.

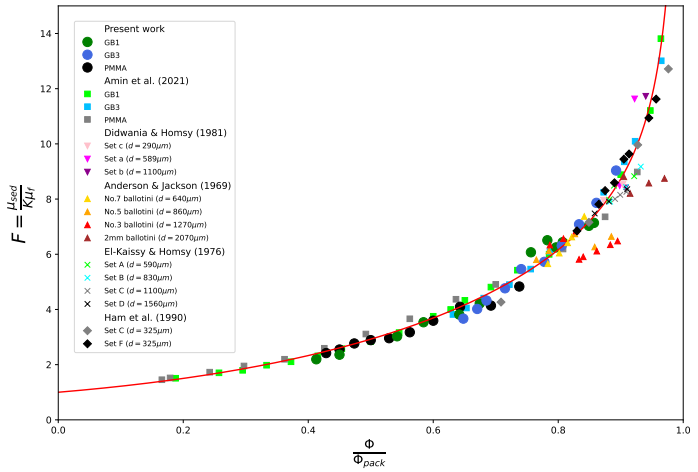

FIG. 6. Experimental values of $F = \mu_{sed}/(K\mu_f)$ determined using values of K given in Fig. 7. The curve corresponds to empirical relation (4).

The corresponding values of K are plotted in Fig. 7 as a function of St_0. Expression (4) exhibits a classic power-law divergence, $(1-\frac{\Phi}{\Phi_{pack}})^{-2/3}$, when approaching Φ_{pack}. However, this asymptotic behavior is not relevant at low concentrations, where an exponential increases, $\exp(1.9\frac{\Phi}{\Phi_{pack}})$, is observed. Adding a quadratic factor, $(\frac{\Phi}{\Phi_{pack}})^2$, to the high-concentration term ensures a smooth transition between these two behaviors.

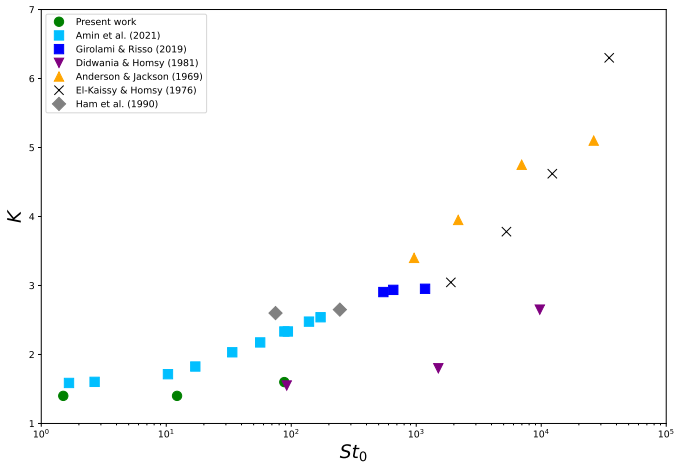

FIG. 7. Values of K used to fit Eq. (4) on experimental data plotted in Fig. 6. Dark blue squares correspond volcanic ash or FCC particles fluidized by a hot dry air from [11].

First of all, Fig. 6 shows that most of the data can be collapsed on the master curve (4) found by [3] despite the variety of physical parameters covered by the different studies. As already discussed, the slight discrepancies with our data are due to fluctuations in the incoming flow. Regarding other previous studies, effects of the confinement and Reynolds number are expected according to the values of w/d and Re reported in Table II. However, only data of Ref. [8] for particles larger than 860 μm and at large concentration are incompatible with the master curve, since they do not follow the expected divergence as Φ tends toward Φ_{pack}. This suggests that the separation, noted by [3], between the effect of the concentration, accounted for by a unique function $F(\Phi/\Phi_{pack})$, and other parameters, accounted by coefficient K, may have a more general validity.

Unlike F, the values of K shown in Fig. 7 are more dispersed. If the reference results for liquid-solid [3] (light blue squares) and gas-solid [11] (dark blue squares) fluidized beds can be described by a function of only St_0, the results of other studies do not collapse on the same curve. The larger K, the smaller U_f and the greater the drag force on the particles and the sedimentation viscosity. With the present results (green circles), K is also an increasing function of St_0, but its values are much less. This enhanced settling may be attributed to the formation of clusters that decreases the drag as it is observed in bubble swarms [13]. It is difficult to draw conclusions for the cases measured under confined conditions,

which may also imply a non-small Reynolds number. The results of Didwania & Homsy [10] (upside-down triangles), performed with beads of 290 to 1100 μm at Re between 1.7 to 170 in a two-dimensional column with a gap of 31.5 mm, also show K smaller than those of Ref. [3, 11] and coincide with the present GB3 at $St_0 = 92$. The results of Anderson & Jackson [8] (triangles), with beads of 640 to 2070 μm in a cylindrical column of 7 mm or 38.1 mm diameter at Re between 5 and 84, show large values of K, from 3.4 to 5. The results of Homsy [9] (crosses), with beads of 590 to 1560 μm in a pipe of 24.5 mm at Re between 6 and 80, show values of K around 3 for St_0 less than 10^4 and of 5.5 beyond. Finally, the results Ham et al. [4] (diamonds), involving beads of 325 μm at Re less than 2 in a cylindrical column of 12.7 mm, are rather close to the results of Ref. [3]. Confinement is expected to increase K since it is known that it causes an increase in drag. All results above the blues squares ([3, 11]) are influenced by confinement. On the other hand, results below the blues squares involve a dominant effect of Reynolds number (inverse triangles from [10]) or inlet condition (circles from this study), which is thereby observed to cause a reduction in drag.

At this stage, we conclude that it is only when U_f is equal to U_{sed} and in the absence of confinement ($w/d \gg 1$) that U_f depends only on the properties of the fluid, those of the particles, concentration and gravity. However, in most of the cases, the main differences turn out to be embedded in the values of K while the evolution of $\mu_{sed}/(K\mu_f)$ can be described by a unique function $F(\frac{\Phi}{\Phi_{pack}})$.

	d($10^{-6}m$)	w/d	ϕ_{pack}	$\phi^* = \phi_s/\phi_{pack}$	$f(Hz)$	$U_f(m.s^{-1})$	$\Delta\rho(kg.m^{-3})$	St_0	$Re = \frac{\rho_f U_f d}{\mu_f}$
Didwania & Homsy (1981) [10]									
Set c	290	29	0.64	0.903	1.6	0.002	1903	92	1.73
				0.872	2.3	0.003			2.60
Set a	589	109	0.63	0.922	1.5	0.0011	2990	1502	25.9
				0.898	2.2	0.016			37.7
Set b	1100	53	0.62	0.940	1.6	0.026	2990	9738	114
				0.907	2.3	0.038			169
Anderson & Jackson (1969) [8]									
No.7 ballotini	640	19.84	0.60*	[0.783, 0.841]	1.25	[0.012, 0.008]	1950	961	[5.50, 7.68]
No.5 ballotini	860	14.76, 29.53	0.60*	[0.765, 0.885]	1.1, 1.5	[0.017, 0.013]	1860	2166	[11.5 , 15.2]
No.3 ballotini	1270	10, 20	0.60*	[0.786, 0.894]	0.75	[0.029, 0.024]	1860	6976	[31.2, 36.4]
2mm ballotini	2070	12.27, 18.40	0.60*	[0.905, 0.970]	1.1	[0.042, 0.037]	1700	26297	[77.0, 83.6]
El-Kaissy & Homsy (1976) [9]									
Set A	590	38	0.65	[0.881, 0.921]	[0.6, 1.4]	[0.0112, 0.0095]	2991	1892	[6.27, 7.40]
Set B	830	27	0.63	[0.883, 0.932]	[0.5, 1.6]	[0.0186, 0.0149]	2991	5268	13.8, 17.3]
Set C	1100	20	0.61	[0.890, 0.909]	[0.8, 0.9]	[0.0276, 0.0261]	2991	12264	[32.1, 34.0]
Set D	1560	15	0.61	[0.858, 0.910]	[0.7, 1.5]	[0.0447, 0.0373]	2991	34982	[65.1, 78.0]
Ham et al. (1990) [4]									
Set C	325	24	0.59	[0.708, 0.976]	[0.05, 0.29]	[0.0011, 0.0045]	1490	75	[0.358, 1.46]
Set F	325	24	0.60	[0.830, 0.957]	[0.10, 1.50]	[0.0025, 0.0050]	3140	245	[0.812, 1.63]
Present study									
GB1	160	1250	0.59	[0.413, 0.854]	[0.1, 0.4]	[0.0011, 0.0060]	1502	12	[0.19, 1.1]

.

TABLE II. Physical parameters and ranges of operating conditions of previous experimental investigations that are compared with the present work. * Values of Φ_{pack} are not available in Ref [8] and have been set to 0.6.

IV. TIME OSCILLATIONS AND SPATIAL DEFORMATION OF THE SURFACE

In this section, we examine the oscillations of the bed surface, $h'(x,t)$. We are interested to check whether there is a relation between the average sedimentation velocity and the characteristics of these fluctuations. For that reason, we focus on GB1 particles since a transition is observed in the difference between U_f and U_{sed} around $\Phi/\Phi_{pack} = 0.6$ in Fig. 5.

Fig. 8 presents the variance of the bed fluctuations computed by averaging over time at location x, $\sigma^2(x) = \overline{h'^2}(x)$. The cases are ordered from left to right and from top to bottom in decreasing order of Φ/Φ_{pack}, which means in increasing order of bed expansion E and sedimentation velocity U_f. Location $x = 0$ corresponds to a wall, while $x = 100$ mm is the middle of the column (marked by a thin dash line). At large concentrations ($\Phi/\Phi_{pack} \gtrsim 0.6\cdot$), the variance σ^2 is almost flat, except for a small increase when approaching the wall, which is localized below $x_{low} = 40$ mm (marked with a thick dashed line) and is more pronounced at smaller expansions. At $\Phi/\Phi_{pack} = 0.541$, σ^2 starts to increase near the wall, and for $\Phi/\Phi_{pack} \leq 0.449$ σ^2 is no more constant in the central region ($x \geq x_{low}$), which means

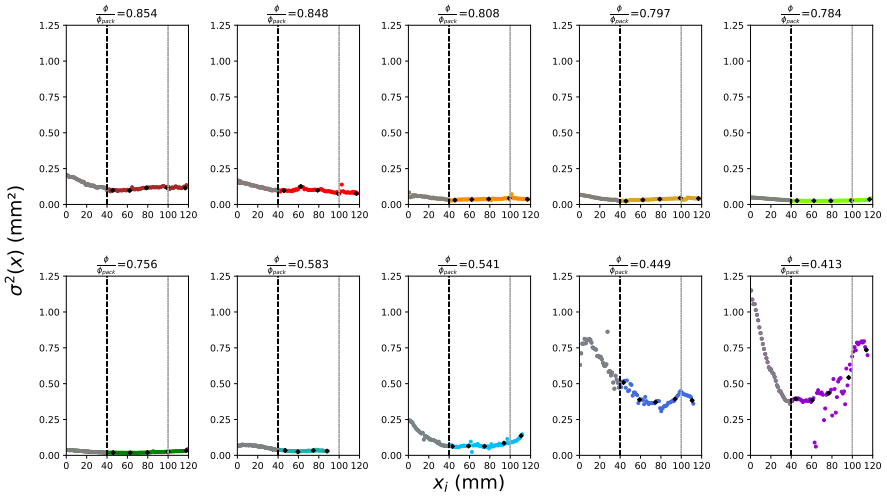

FIG. 8. Variance of the bed fluctuations, $\sigma^2(x) = \overline{h'^2}(x)$, as a function of location x at various concentrations Φ/Φ_{pack}.

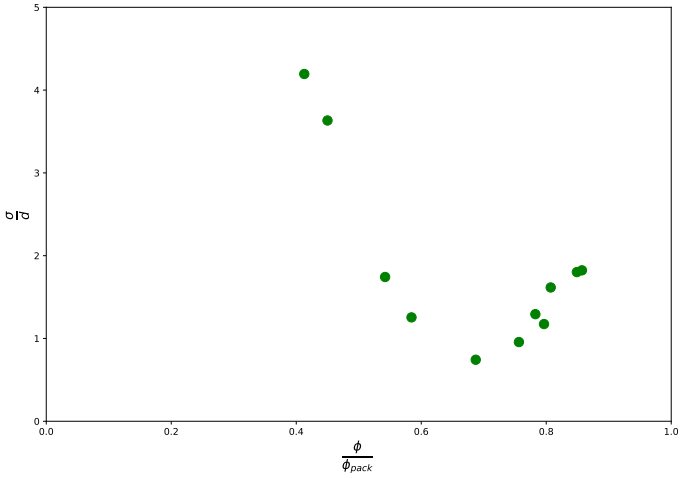

FIG. 9. Standard deviation of the bed height normalized by the particle diameter, computed by time and space averaging in the central region of the column.

that the surface is nowhere flat. Another important observation is that neither average nor the fluctuating sedimentation velocity disappears at the wall, whereas the velocity of the suspending fluid does. This proves the existence of a significant slip velocity of the particles at the walls, which seems to be a common feature of concentrated suspensions either at negligible [14] or large [15] Reynolds number.

Fig. 9 shows the standard deviation of the bed height σ normalized by the particle

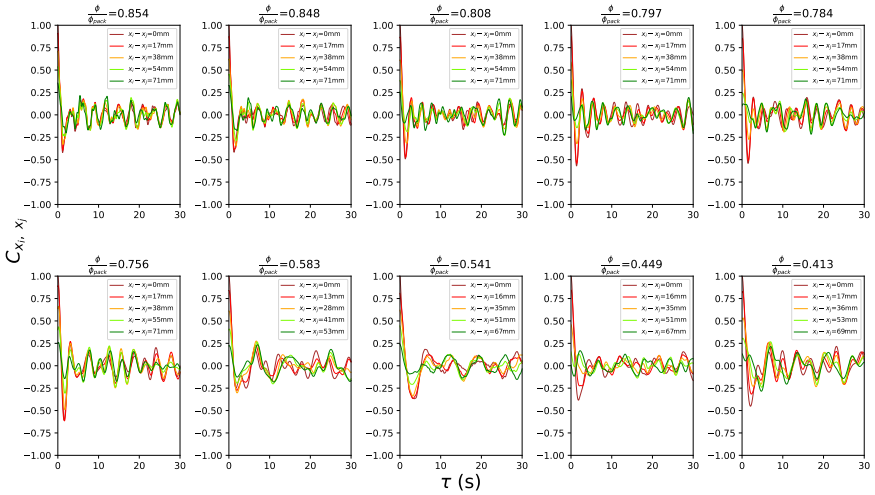

FIG. 10. Time cross-correlation of the surface height between two points, x_i and x_j.

diameter d, computed by averaging over both time and space in the central region ($x_{low} \leq x \leq x_{max}$). We again see a transition around $\Phi/\Phi_{pack} \approx 0.6$, where the oscillation amplitude is minimum ($\sigma = 0.74d$). Decreasing the concentration, σ steeply increases to reach a value of $4.19d$ at $\Phi/\Phi_{pack} = 0.41$. Increasing the concentration above this point, σ increases moderately to reach a value of $1.82d$ at $\Phi/\Phi_{pack} = 0.854$.

We now want to know whether the surface fluctuations at different locations are synchronized with each other or not, an information that is not contained in the single-point measurements. In particular, the fact that a variance profile represented in figure 8 is flat, as is the case at intermediate concentrations, does not guarantee that the surface is flat at a given instant. Cross-correlation is a good tool to gain insight into this matter. We define the time correlation between two points x_i and x_j of the surface,

$$C_{x_i,x_j}(\tau) = \frac{\overline{h'(x_i,t)h'(x_j,t+\tau)}}{\sqrt{\overline{h'^2(x_i)}}\sqrt{\overline{h'^2(x_j)}}}\,. \tag{5}$$

Fig. 10 presents $C_{x_i,x_j}(\tau)$ for pairs of points located in the central region ($x_{low} \leq x \leq x_{max}$). The point x_i is fixed to a location near the end x_L of the measurement window, while x_j is moved to several locations, so that the distance between them is varied from zero to approximately 60 mm. All curves show a dominant frequency, indicating the existence of a deterministic mechanism that will be analyzed in the next section. For now, we note that when the oscillations displayed by the cross-correlations obtained at two different x_j for a given concentration are in phase, we can conclude that the motions of these two points are

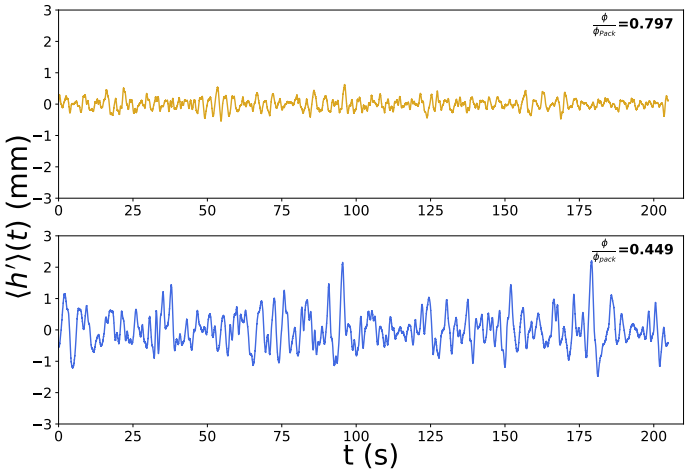

FIG. 11. Time evolution of the spatially-averaged bed height for the same cases as in Fig. 4.

synchronized. Such a synchronization is observed for $\Phi/\Phi_{pack} \gtrsim 0.6$ up to time delays larger than 20 s. The synchronization degrades at smaller concentrations. At $\Phi/\Phi_{pack} \leq 0.449$, even the first oscillations can be in phase opposition, indicating a severe de-synchronization of the fluctuations. Visual inspection of the movies confirms these conclusions. At low expansion, the surface is observed to oscillate in the vertical direction as a whole. At large expansion, sloshing motion develops, breaking the synchronization between adjacent points.

V. VERTICAL SURFACE OSCILLATIONS AND TRAVELING WAVES

From now, we focus on time fluctuations and ignore any spatial heterogeneity by considering the bed height, $\langle h \rangle(t)$, which is spatially averaged over the central part of the column ($x_{min} \leq x \leq x_{max}$). Then, we define its time fluctuations, $\langle h' \rangle(t) = \langle h \rangle(t) - \overline{\langle h \rangle(t)}$, by removing their time average $\overline{\langle h \rangle(t)}$.

Fig. 11 presents two examples of time evolution $\langle h' \rangle(t)$. Compared to the local signals shown in Fig. 4, the spatial average of the height contains less high frequencies and thus appears less noisy. However, it has a similar low frequency content except that the effect of sloshing occurring at small concentration is attenuated, making it suitable for analyzing the main features of the vertical oscillations. The presence of a dominant frequency in $\langle h' \rangle(t)$ is visible at all concentrations. It can be better distinguished from the stochastic part of the signal by considering the autocorrelation function, $C(\tau) = \frac{\overline{\langle h' \rangle(t) \times \langle h' \rangle(t+\tau)}}{\overline{\langle h' \rangle^2(t)}}$, which is presented in Fig. 12. For all volume fractions considered, $C(\tau)$ shows a peak at the origin that

ends before $\tau = 1$ s, followed by smooth oscillations with one main and a few secondary frequencies which do not de-correlate in more than 50 s. This means that the high-frequency content accounted for by the initial peak corresponds to random fluctuations, whereas the regular low-frequency oscillations are associated with a deterministic mechanism. The magnitude of the correlated oscillations in $C(\tau)$ is in between 0.11 and 0.13 at $\Phi/\Phi_{pack} \geq 0.808$ and approximately 0.17 at lower concentrations. While the total energy σ^2 of the fluctuations varies by a factor of 30 between the highest and lowest values (Fig. 9), the relative contribution of the deterministic oscillations does not change much.

The dominant frequencies are better determined in the spectral domain. Fig. 13 shows the power spectral density of $\langle h' \rangle(t)$ computed by the periodogram method based on the Fourier transform of the time signal. Its characteristics vary with concentration. In any case, the largest frequencies detected are less than 3 Hz, with a dominant frequency of less than 0.43 Hz. These values are very small compared to the pump's 40 Hz cyclic frequency, allowing us to conclude that they are independent of any pump-induced effects. At lower expansions ($\Phi/\Phi_{pack} \geq 0.797$), the spectrum extends between 0.1 and 1 Hz with a main peak around 0.4 Hz and a significant secondary peak at a frequency below 0.3 Hz. At intermediate concentrations ($0.687 \geq \Phi/\Phi_{pack} \geq 0.784$), where the energy of the fluctuations is the lowest, the spectrum has shifted slightly towards lower frequencies and shows up to 3 secondary peaks. At larger expansions ($\Phi/\Phi_{pack} \leq 0.583$), the highest peak, located in between 0.1 and 0.2, becomes very dominant.

Fig. 14 shows the frequency f of the dominant harmonic as function of Φ/Φ_{pack}. It has been normalized by the particle diameter and fluidization velocity in the form fd/U_f to allow comparison with other systems of fluid and particles. The results of previous studies reported here correspond to frequency measurements of concentration waves traveling through the suspension. They all concern low expansions close to the minimum fluidization velocity ($\Phi/\Phi_{pack} \geq 0.8$), with the exception of one measurement from Ham et al. [4] at $\Phi/\Phi_{pack} = 0.7$. On the other hand, our results cover the range $0.40 \leq \Phi/\Phi_{pack} \leq 0.85$. We did not take any measurement for $\Phi/\Phi_{pack} > 0.85$ because satisfactory fluidization could not be achieved throughout the column at such high concentrations using our system. The range of concentrations Φ/Φ_{pack} studied in common by the literature and the present work therefore lies between 0.7 and 0.85. In this range, our measurements agree fairly well with those of previous studies, particularly with those of Ham et al. [4] who considered particles

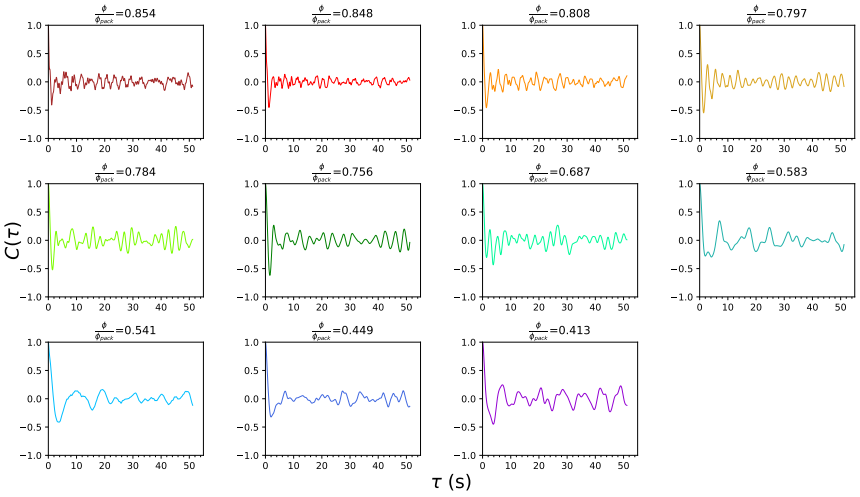

FIG. 12. Fig. Autocorrelations of the bed-height time evolution for various particle concentrations.

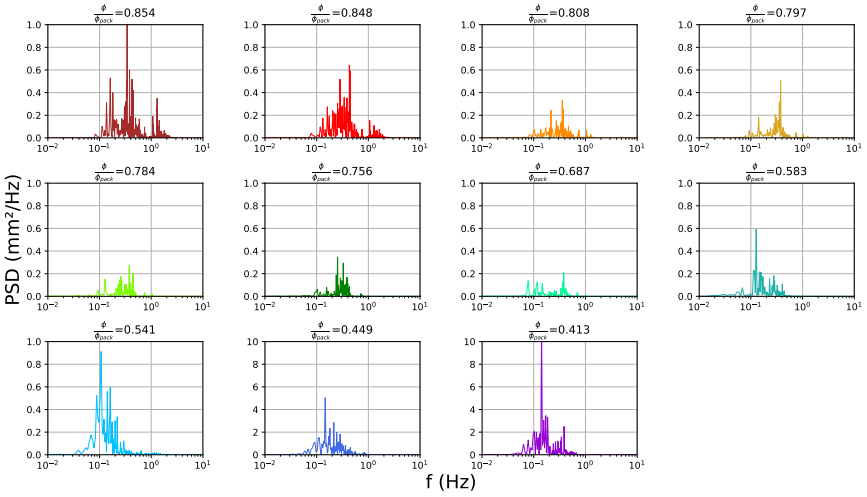

FIG. 13. Fig. Power spectral density of the bed-height time evolution for various particle concentrations.

with similar properties. By taking all the results into account, we can describe a wide concentration range, revealing three stages as Φ/Φ_{pack} increases. For $0.4 \leq \Phi/\Phi_{pack} \leq 0.6$, the normalized frequency slightly increases from approximately 3×10^{-3} to 7×10^{-3}. Above $\Phi/\Phi_{pack} = 0.6$, it jumps to a value greater than 10^{-2} and goes on increasing to reach a maximum for a value of Φ/Φ_{pack} between 0.8 and 0.9. Then, the frequency strongly decreases while the system is approaching the packing state. Although system parameters, including confinement and inlet conditions, strongly influence fluidization velocity, the evolution of the normalized frequency turns out to be less sensitive to these parameters.

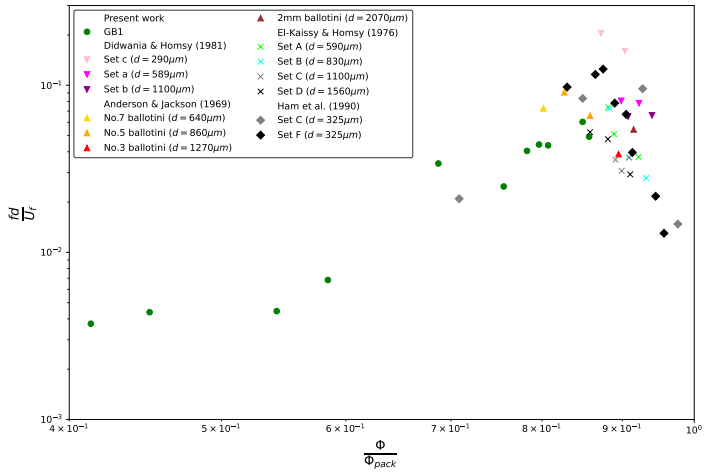

FIG. 14. Dimensionless dominant oscillation frequency as a function of the concentration.

The dynamics of fluidized beds is a long-standing subject and the existence of upward concentration waves passing through them is well known [16]. The theoretical equations for plane waves propagating in an unconfined bed have been established by considering perturbations of the mass and momentum balances around the homogeneous state by Anderson and Jackson in 1968 [17] and then by Batchelor in 1988 [1], who followed a more rigorous approach. Linear analysis showed that these waves can give rise to convective or absolute instability [18]. This waves are a first step toward a global destabilization of a homogeneous fluidized bed. They can be followed by a secondary instability that breaks the one-dimensional structure, which has been described theoretically [5, 19–21] and observed experimentally [6].

Following Batchelor [1], the wave dynamics involve several physical parameters, such as the diffusivity, drag and added-mass coefficients, and velocity variance of the particles. How to relate these quantities to the control parameters of the bed is unfortunately not known. From their values, it is possible to determine Q, the effective bulk elastic modulus of the suspension divided by the particle mass per unit volume. Two kinds of concentration waves can exist separately according to the operating conditions. Firstly, the kinematic wave results from the transport equation of the particle concentration and has a propagation velocity,

$$c_{kw} = \Phi \frac{\mathrm{d}U_f}{\mathrm{d}\Phi}\,. \tag{6}$$

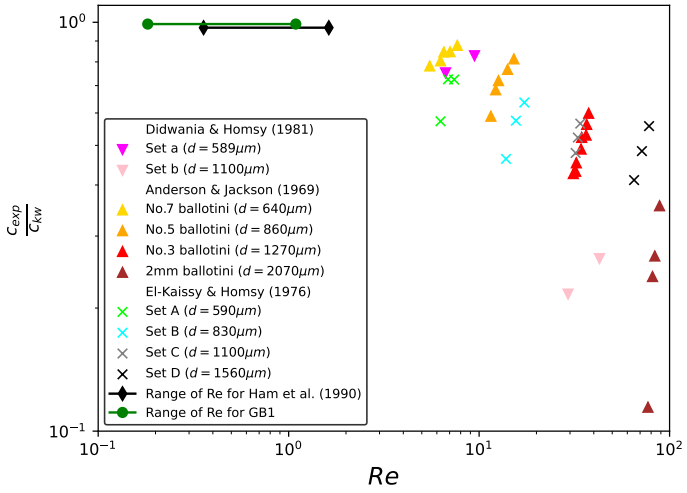

FIG. 15. Ratio of the propagation velocity measured in the experiments and that of the kinematic waves calculated using Eq. (6). (For Ham et al (1990) and the present study, the ratio has been arbitrarily fixed to unity and is only represented to indicate the Reynolds range).

Secondly, the dynamic wave results from the momentum equation, whose propagation velocity is

$$c_{dw} = Q^{1/2} \,. \tag{7}$$

In this study, interface fluctuations are interpreted as the arrival of upward concentration waves at the top of the bed, which is confirmed by the good agreement with previous wave propagation studies in terms of frequency. Since coherent oscillations are observed over long periods of time, we can conclude that our bed is unstable with respect to planar waves. The question of the type of waves observed here remains open. Observation of the bed surface does not allow us to measure the wave velocity. We will therefore rely on the results of previous work.

The experimental propagation wave velocity, c_{exp}, has been measured in Refs. [8–10]. The kinematic wave velocity c_{kw} is calculated by applying Eq. (6) to the relation between the fluidization velocity and the particle concentration measured in each experiment. Fig. 15 shows the ratio c_{exp}/c_{kw} as a function of the particle Reynolds number. The velocity c_{exp} has not been measured by Ham et al (1990). In their case, as in ours, the ratio c_{exp}/c_{kw} has been fixed at one and only plotted to indicate the range of Re. A clear trend emerges from the available data. The lower Re, the less scatter for a given series and the closer c_{exp}/c_{kw}

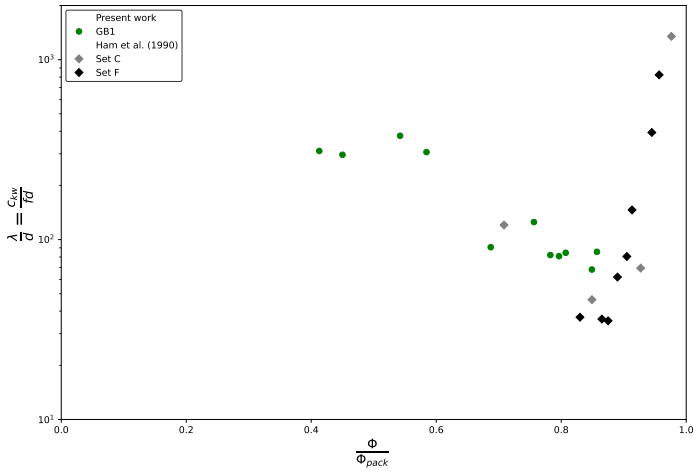

FIG. 16. Wavelength of the propagating waves as a function of the particle concentration.

is to unity. The smallest available value of Re is 5, where c_{exp}/c_{kw} is in between 0.8 and 1. Since the range of Re is between 0.35 and 1.8 in Ham et al (1990) and between 0.19 and 1.1 in this study, we will assume that $c_{exp}/c_{kw} = 1$ in both cases.

We are therefore justified as considering that our fluidized bed and that of Ham et al (1990) are operated in the same regime, where coherent oscillations of the concentration are dominated by kinematic waves. Knowing the wave velocity, we can compute the wavelength as $\lambda = \frac{c_{kw}}{f}$. Fig. 16 shows the normalized wavelength $\frac{\lambda}{d}$ as a function the normalized concentration Φ/Φ_{pack}. The results of the two studies coincide in the region where their concentration ranges overlap. The wavelength reaches a minimum of a few tens of d around $\Phi/\Phi_{pack} = 0.85$. From this minimum, the measurements of Ham et al (1990) show that λ rises sharply to exceed $10^3 d$ as Φ approaches the onset of coherent oscillations, just before the packing state. This trend is expected from the linear theory, which predicts that long wavelengths are the most unstable. In the other direction, λ also increases as the bed expands until it reaches a plateau around $350d$ for $\Phi/\Phi_{pack} < 0.6$, which corresponds to the region where the wave loses its one-dimensional character and the surface begins to slosh.

At this stage, it is important to recall that the range of concentrations studied in common by the literature and the present work is $0.7 \leq \Phi/\Phi_{pack} \leq 0.85$. Consequently, we cannot determine whether the sharp increase in wavelength when approaching the minimum fluidization velocity observed by Ham et al. (1990) is affected by confinement. Moreover, the

decrease in frequency and the increase in wavelength we observed when decreasing Φ_s/Φ_{Pack} below 0.7 is a new phenomenon that cannot be compared with previous results for confined flows.

It is now interesting to discuss the bed homogeneity in the light of these results. Since the time correlation (Fig. 12) and spectrum (Fig. 13) of height fluctuations have shown that the time scales of all coherent structures are of the same order, the wavelength λ can be interpreted as the scale of the suspension heterogeneities in the vertical direction. As shown in figure 16, λ is much larger than d, so the suspension can be considered statistically homogeneous at the particle scale. The picture is different if we look at the scale of the whole bed. The column of Ham et al (1990) is a cylinder a diameter w of 78 mm and the bed height h is between 0.4 and 0.6 m depending on the expansion. Thus, λ is always greater than the width of the bed ($1.5 \leq \lambda/w \leq 60$), but remains less than a tenth of the height of the bed, except for $\Phi/\Phi_{pack} > 0.9$ where it approaches unity. In this study, the sides of the rectangular column (w_1 =200 mm, w_2 =300 mm) are comparable to the bed height ($210 \leq h_{mid} \leq 440$ mm). Therefore, λ is lower than a tenth of all the bed dimensions at moderate expansion ($\Phi/\Phi_{pack} > 0.6$). However, at larger expansions, the wavelength reaches $\lambda/h_{mid} \approx 0.15$ and $\lambda/w \approx 0.25$. In addition, we know from the images in Fig. 2 and the analysis of section IV, that the bed surface is no longer flat or moving vertically as a whole during such expansions. It is therefore likely that the overall destabilization of the bed at high expansions occurs when the size of the heterogeneities associated with the rising waves reaches the dimension of the column.

VI. CONCLUSION

Experimental studies of a liquid-solid fluidized bed were carried out under unconfined conditions. Due to the huge number of interfaces present in the column, it was hardly possible to measure concentration and velocity inside the suspension, and we limited ourselves to measurements of bed surface motion. Both the fluidization velocity, U_f, that prevents the suspension from settling and the sedimentation velocity, U_{sed}, undergone by the particle when they settle in a fluid at rest were measured. It is possible that U_f and U_{sed} match because the particles are observed to slip along the lateral walls, which therefore allows the average velocity profiles of the particles to remain flat in both cases. However, this matching

requires that the flow injected in the fluidization case does not bring any disturbances that significantly increase the particle random agitation compared to the sedimentation case. When this is the case, U_f becomes greater than U_{sed}.

Comparisons of sedimentation velocity were made with previous work dealing with both unconfined and confined systems, at low to moderate Reynolds numbers. It turned out that, when normalized by $U_0(1-\Phi)$ (where U_0 is the Stokes falling velocity of an isolated particle), all values of U_f collapse to a single master curve $1/(K \times F(\Phi/\Phi_{pack}))$. In a sense, K plays the same role as the U_i (the value of U_f in the dilute limit) in Richardson-Zaki inspired correlations, while F plays that of exponent n. Whereas the function F remains the same, K varies according to Stokes number, Reynolds number, inlet conditions and confinement ratio.

The fluctuations of the fluidized bed surface have been studied in detail for a particle Reynolds number below one. They include uncorrelated high frequencies associated with the suspension microstructure and low frequency coherent oscillations involving a few harmonics. These coherent oscillations are the signature of the arrival at the bed surface of ascending concentration waves, which are known to develop in fluidized beds. The main oscillation frequency f is in fairly good agreement with previous studies. Unlike sedimentation velocity, it seems to be essentially determined by the physical properties of the fluid and particle system, and more robust to confinement and inlet conditions. It increases slowly at first, then steeply with the concentration Φ to reach a maximum between 0.8 and $0.9\Phi_{pack}$, before decreasing sharply as the system approaches the packing state.

Results from the literature suggest that in the range of parameters concerned, where inertia is moderate, the propagation velocity is that of kinematic waves, c_{kw}. Using the theoretical expression (7), c_{kw} is calculated from the experimental sedimentation law $U(\Phi/\Phi_{pack})$. This allows us to determine the wavelength, $\lambda = \frac{c_{kw}}{f}$, in our case and that of Ham et al (1990) [4], which has similar parameters. The wavelength has a general U-shape, with a minimum around $\Phi/\Phi_{pack} = 0.85$, from which it increases as the concentration tends towards both the packing state and the dilute regime. Considering λ as the size of bed heterogeneities lead to the following conclusions. On the one hand, the increase of λ at small expansions can be related to the divergence of the correlation length between particle locations as the system approach the jamming transition. On the other hand, the increase at large expansions can set the limit for the overall homogeneity of the fluidized bed as λ ceases to be

small compared to the column dimensions, in a system where these dimensions are much larger than the particle size.

ACKNOWLEDGMENTS

This study was supported by the Region Centre-Val de Loire through the Contribution of "Academic Initiative": RHEFLEXES/ 2019-00134935.

---

[1] G. K. Batchelor, A new theory of the instability of a uniform fluidized bed, J. Fluid Mech **193**, 75 (1988).

[2] J. Richardson and W. N. Zaki, Sedimentation and fludization : part 1, Trans. Instn Chem. Engrs **32**, S82 (1954).

[3] A. Amin, L. Girolami, and F. Risso, On the fluidization/sedimentation velocity of a homogeneous suspension in a low-inertia fluid, Powder Technology **391**, 1 (2021).

[4] J. Ham, S. Thomas, E. Guazzelli, G. Homsy, and M.-C. Anselmet, An experimental study of the stability of liquid-fluidized beds, International Journal of Multiphase Flow **16**, 171 (1990).

[5] G. K. Batchelor, Secondary instability of a gas-fluidized bed, Journal of Fluid Mechanics **257**, 359 (1993).

[6] P. Duru and E. Guazzelli, Experimental investigation on the secondary instability of liquid-fluidized beds and the formation of bubbles, Journal of Fluid Mechanics **470**, 359 (2002).

[7] E. Alméras, F. Risso, o. Masbernat, and R. O. Fox, Statistics of velocity fluctuations in a homogeneous liquid fluidized bed, Physical Review Fluids **6**, 034301 (2021), publisher: American Physical Society.

[8] T. Anderson and R. Jackson, Fluid mechanical description of fluidized beds. Comparison of theory and experiment, Ind. Eng. Chem. Fundam. **8**, 137 (1969).

[9] M. M. El-Kaissy and G. M. Homsy, Instability waves and the origin of bubbles in fluidized beds. part 1. experiments, Int. J. Multiphase Flow **2**, 379 (1976).

[10] A. K. Didwania and G. M. Homsy, Flow regimes and flow transitions in liquid fluidized beds, int. J. Multiphase Flow **7**, 563 (1981).

[11] L. Girolami and F. Risso, Sedimentation of gas-fluidized particles with random shape and size,

Physical Review Fluids **4** (2019).

[12] L. Girolami, F. Risso, A. Amin, L. Rousseau, A. Bondesan, and S. Bonelli, Sedimentation of short-lived fluid-solid suspensions, Physics of Fluids **36**, 113308 (2024).

[13] V. Garbin, D. Bothe, G. Brenn, C. M. Casciola, C. Colin, M. Marengo, F. Risso, G. Tryggvason, and D. Lohse, Bubbles and bubbly flows, International Journal of Multiphase Flow , 105240 (2025).

[14] S. Roman, S. Lorthois, P. Duru, and F. Risso, Velocimetry of red blood cells in microvessels by the dual-slit method: Effect of velocity gradients, Microvascular Research **84**, 249 (2012).

[15] A. Amin, L. Girolami, and F. Risso, Fall of a large sphere in a suspension of fluidized particles, Physical Review Fluids **7** (2022).

[16] R. Jackson, *The dynamics of fluidized particles*, Cambridge monographs on mechanics (Cambridge University Press, Cambridge ; New York, 2000).

[17] T. Anderson and R. Jackson, A fluid mechanical description of fluidized beds. stability of the state of uniform fluidization., Ind. Eng. Chem. Fundam. **7**, 12 (1968).

[18] M. Nicolas, J. M. Chomaz, and E. Guazzelli, Absolute and convective instabilities of fluidized beds, Phys. Fluids **6**, 3936 (1994).

[19] J. M. Nitsche and G. K. Batchelor, Instability of stationary unbounded stratified fluid, Journal of Fluid Mechanics **227**, 357 (1991).

[20] J. M. Nitsche and G. K. Batchelor, Instability of stratified fluid in a vertical cylinder, Journal of Fluid Mechanics **252**, 419 (1993).

[21] J. M. Nitsche and G. K. Batchelor, Expulsion of particles from a buoyant blob in a fluidized bed, Journal of Fluid Mechanics **278**, 63 (1994).